EPI-ILLUMINATION OPTICAL DESIGN FOR FLUORESCENCE POLARIZATION MEASUREMENTS IN FLOW SYSTEMS

W. G. EISERT, *Gesellschaft für Strahlen-und Umweltforschung, Institut für Angewandte Physik, Abteilung für Ökologische Physik, Hannover*
W. BEISKER, *Universität Hannover, Institut für Biophysik, 3000 Hannover 21, West Germany*

ABSTRACT An epi-illumination design for fluorescence polarization measurements is introduced in flow cytometry with the optical axis orthogonally aligned to the cell stream. Various optical components and designs are discussed with respect to their influence on polarization measurements. Using the epi-configuration, paired measurements with the direction of polarization of the exciting light changed orthogonally are proposed for the compensation of system anisotropies and electronic mismatch. Large aperture corrections are employed for the excitation as well as for the emission pathway. Additional parameters such as fluorescence at 90°, multiangle light scattering, and high precision cell-sizing by internally calibrated time of the flight measurements, as described previously, remain available with the design proposed here. Fluorescent latex microspheres, stained intracellular DNA, and algae have been used to test performance.

INTRODUCTION

In the past, measurements of the polarization of fluorescence emission have been used to probe the geometrical relationship of the fluorescent molecule to its environment. This technique has been employed primarily in polymer science to investigate either orientation in frozen media, molecular mobility in isotropic media (15, 16), or concentration effects (8). Polarization measurements of fluorophores in cell biology, however, are influenced by a much larger number of factors, such as the chemical and physical microenvironment (1, 4, 5, 7), including chemical reactions and energy transfer (6, 15, 16). Probing the cytoplasmic microenvironment in lymphocytes by fluorescein-diacetate incubation has been proposed as a tool for cancer screening (4, 5, 18). A number of measurements on single cells and in cell suspensions were followed by experiments reproducing these results with a flow system (12, 21, 22). Fluorescence measurements using a flow cytometer exhibit the advantage of virtually no background fluorescence, and therefore higher signal to noise ratio, and of data evaluation on a cell-by-cell basis. However, care must be taken when comparing results of low intensity excitation using conventional light sources and cell suspensions in cuvettes with data of laser flow cytometry using the comparatively high excitation intensity of a focused laser source. Recent studies on the angular distribution of fluorescence emission of particles showed the strong influence of light scattering in excitation as well as fluorescence emission (17, 19). This seems to play an important role in highly structured particles and cells. The smallest deviation from the ideal fluorescence without scattering is found for fluorescence emission either in the

forward or the backward direction with respect to the excitation. To avoid experimental difficulties by the strong excitation beam, in detecting fluorescence emission in the direction of the excitation, we chose the backward direction known as epi-illumination in conventional microscopy.

MATERIALS AND METHODS

Most flow systems being used for fluorescence polarization measurements have used a stream-in-air flow and have the direction of fluorescence detection aligned perpendicular to the excitation and flow axes. In contrast to conventional bulk measurements on solutions or suspensions, flow cytometer systems use two independent detector channels for measuring the perpendicular polarization components of each cell simultaneously. The alignment for equal sensitivity of both detector channels is usually performed by rotating the electric vector of the exciting light parallel to the direction of observation. In this case, both channels, monitoring polarization components of the fluorescence emission in the plane normal to the electric vector of the exciting light, detect unpolarized light and are set to the same response. To minimize possible influences of nonlinear sensitivity and chromatic errors, it has been proposed to use part of the sample for the alignment. Roughly the same total fluorescence intensity and wavelength will be handled for balancing the detector sensitivity as well as for the measurement. This procedure assumes the exciting wave front to be parallel and the detection aperture very small (23). Low fluorescence intensities often make a higher numerical aperture of the detector optic necessary to increase signal to noise ratio. However, emission anisotropy will be underestimated in systems with high numerical apertures. Several approaches have been described to account for the aperture effect of the detectors (2, 8, 20, 23, 24). According to the circular symmetry of the detection aperture of the microscope based equipment, most authors consider a polar or cylindrical coordinate system (2, 23). However, the assumptions mentioned above do not hold for stream-in-air flow cytometry systems (1, 7, 20). Generally the exciting light is focused by cylindrical lenses on the center of the cylindrical fluid stream. This results in an elliptical aperture, i.e., two numerical apertures parallel to the major axes of the ellipse. An additional correction for the excitation becomes necessary. Due to the cylindrical fluid, the emission aperture is also of elliptical cross section, which so far has not been considered in correction algorithms. Therefore, the calculation for correcting excitation as well as emission aperture effects will be derived in cartesian coordinates.

It has been shown that misalignment of the electric vector of the exciting light with respect to the direction of polarization of one detector gives rise to negligible errors (2, 23). Larger contributions are expected by the DC-offset of the electronic signal processors (20), which can be easily measured and corrected during data processing. Light scattering of the exciting beam as well as of the fluorescence emission is known to decrease the observed emission anisotropy (23). This is likely to become a significant contribution of exciting with a focused laser source. Additional complications have to be considered for structured particles and cells. The angular distribution of fluorescence intensities for the two main components of polarization is not uniform (17). Theoretical calculations seem to favor either forward or backward fluorescence detection, as reported here, over measurements at 90° (1, 6, 7, 12, 20, 22) for evaluating emission anisotropy data on highly structured material such as biological cells.

A double sheath flow system with plane viewing windows which has been described for high resolution extinction measurements before (10, 11) avoids cylindrical optical surfaces of stream-in-air designs. Therefore, the aperture correction for the detection pathway will consider a circular aperture, whereas the aperture of the excitation may be considered as circular or elliptical depending on the experimental condition. For circular apertures of the excitation as well as of backward detection path the direction of the electric vector of the exciting beam may be selected arbitrarily. The two orthogonal polarization components of the detection path are than aligned accordingly. A rotation of the polarization of the exciting beam by 90° changes the polarization components being detected from parallel to perpendicular and vice versa. By comparison of the results obtained by the two settings of the excitation polarization, differences in the response of the two detection pathways (optical and electronic portion) can be evaluated and numerically corrected. During actual measurement, the sample is split into two parts, both of which are measured subsequently (within a few minutes) with polarization directions of the exciting light being perpendicularly oriented and without changing amplifier settings. In contrast to the alignment procedure of a 90° design, data of both runs contribute to the result on the sample and improve the statistics of the measurement.

Besides the 90° arrangement for the optical axes and the direction of flow, two different optical arrangements for fluorescence polarization measurements have been described.

Using two independent optical axes for detecting two independent directions of polarization (21) may be of advantage if angles other than 90° between the directions of polarization are of interest. The numerical correction of the values measured need to consider the asymmetries of both polarizations detected at 75° and 105° as proposed in reference 21, with respect to the perpendicular situation. Directing the optical axis of the exciting beam to intersect the air-liquid interface at Brewster's angle (6, 7), favors one direction of polarization to excite the sample. One of the small half axes of the elliptical aperture along the excitation path is reduced at the air-liquid interface. In addition, the main polarization components of the emission are no longer parallel or perpendicular to the major axes of the elliptical detection aperture, which also complicates the numerical correction.

Optical Arrangement

A schematic of the epi-arrangement is shown in Fig. 1. A very flat flow system with a highly focused particle stream has previously been described by us for cell sizing purposes by precise extinction and scattering measurements (9, 10, 11). The apertures are circular in general and the optical system therefore has axial symmetry for excitation and detection. A polarization rotator allows the excitation polarization to be aligned parallel to one polarization component of the calcite crystal, which serves as an analyzing beam splitter. Laser light scattered backwards is blocked by a combination of cut-off and interference filters together with the dichroic mirror. The two photomultipliers are selected to have roughly the same sensitivity.

Excitation Corrections

Various possibilities for disturbing the ideal polarization of the exciting laser beam have to be considered. The laser itself operates in a single transverse mode (TEM_{oo}), which results in a

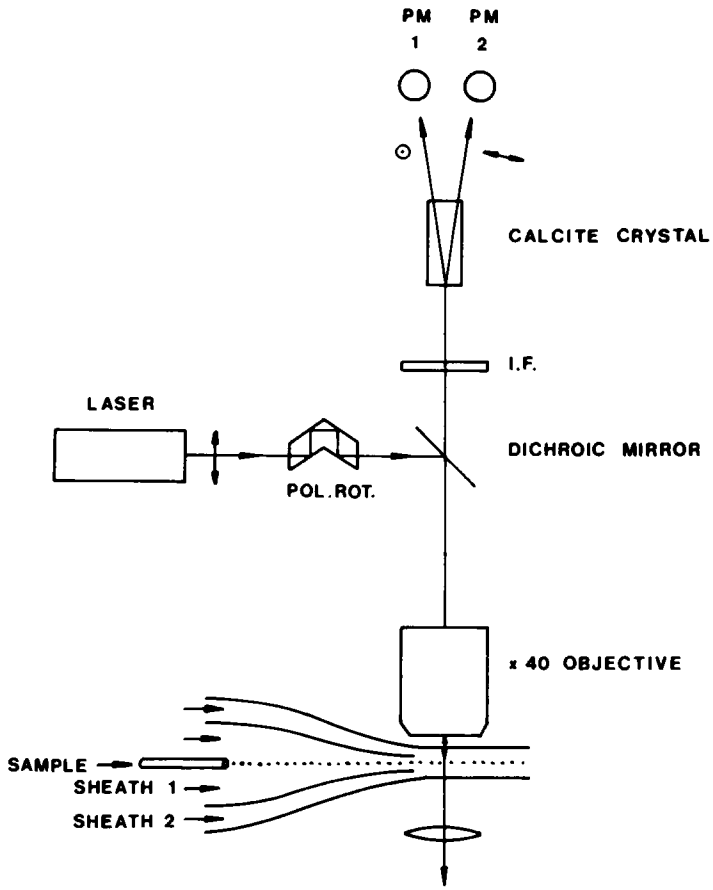

FIGURE 1 Schematic drawing of the epi-illumination fluorescence polarization measurement system. The polarization of the exciting laser may be changed by turning the polarization rotator. After appropriate wavelength selection, the calcite crystal separates the two polarized components of the fluorescence light into two photomultipliers.

Gaussian intensity profile of the beam. However, only single mode operation, i.e., laser oscillation on a single frequency, provides optimized polarization of the laser beam. Generally, in multifrequency, TEM_{oo}-mode operation, linear polarization is maintained by inserting Brewster-windows in the laser cavity. In addition, laser light of high spatial intensity is passed through laser mirrors and optical components. Small optical impurities and dust give rise to scattered light, with an electric vector of different direction than that of the incident light. With careful selection of components and maintenance of the system, these depolarizing effects are neglegible.

A more serious problem arises from all kinds of multilayer coatings in the optical light path especially when their surface is not perpendicular to the optical axis. Dichroic mirrors and beam splitters need to be carefully checked for their transmittance and reflectivity with respect to different directions of polarization. Dichroic beam splitters have to be selected when used close to their cut-off frequency.

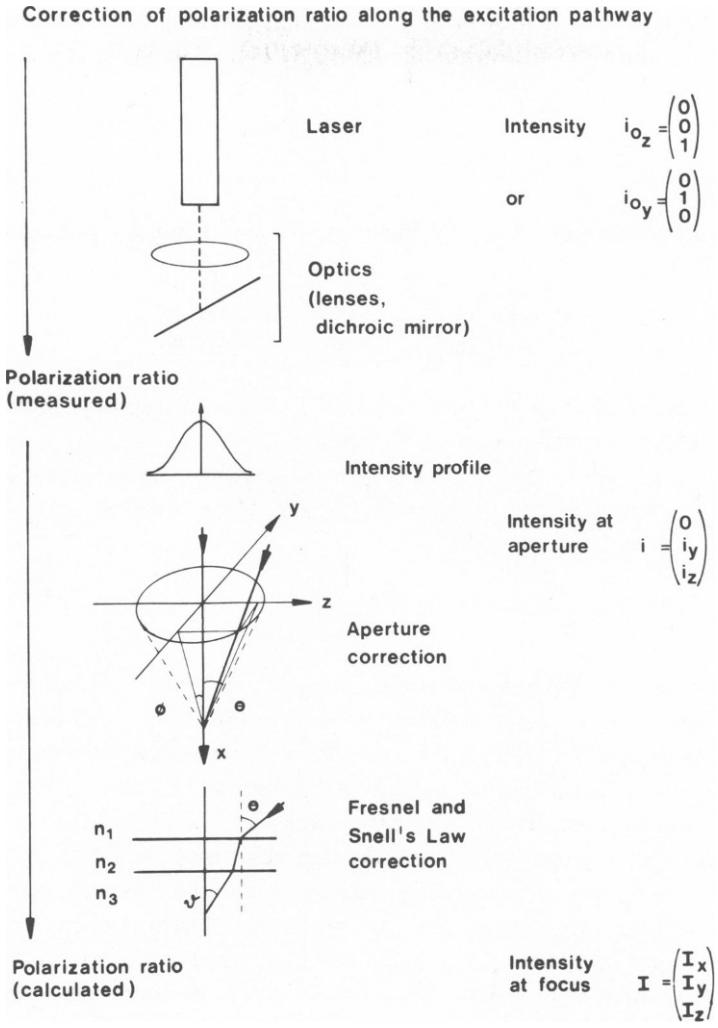

FIGURE 2 Schematic representation of various contributions to the depolarization of the exciting laser beam. The distortion of the ideal polarization i_o due to optical components is measured at the entrance aperture of the objective. Influences of various aperture sizes and cross sections, a nonuniform intensity distribution, as well as the influence of the Fresnel equations and Snell's law are taken into account for the numerical correction. The intensity components at the focus are noted as $I_{x,y,z}$.

Corrections of the polarization ratio along the excitation pathway are summarized schematically in Fig. 2. The x axis is taken as the direction of propagation. The polarization of the laser may be chosen parallel to the z axis or parallel to the y axis. The normalized intensities of the ideally polarized laser beam can be expressed as:

$$\mathbf{i}_{0_z} = \begin{pmatrix} 0 \\ 0 \\ 1 \end{pmatrix} \quad \text{or} \quad \mathbf{i}_{0_y} = \begin{pmatrix} 0 \\ 1 \\ 0 \end{pmatrix},$$

respectively. The depolarization by passing various optical components is determined experimentally at the entrance aperture of the final focusing objective. The normalized intensity is:

$$\mathbf{i} = \begin{pmatrix} 0 \\ i_y \\ i_z \end{pmatrix},$$

assuming a plane wave front, i.e., $i_x = 0$. In our experimental design i was found to be:

$$\mathbf{i}_{l_x} = \begin{pmatrix} 0 \\ 0,05 \\ 0,95 \end{pmatrix} \quad \text{and} \quad \mathbf{i}_{l_y} = \begin{pmatrix} 0 \\ 0,95 \\ 0,05 \end{pmatrix}$$

at the entrance aperture. The intensity profile of the laser was also measured at the same position and found to fit well a Gaussian distribution.

Corrections of the polarization due to focusing and changes in the refractive index of the media then lead to the calculated intensity at the focus which is written as:

$$\mathbf{I} = \begin{pmatrix} I_x \\ I_y \\ I_z \end{pmatrix}.$$

In Fig. 3 the coordinate system and the angle notation, which is used for the following calculations is shown as well as the Gaussian intensity profile of the laser beam.

Different directions of excitation will be considered as projection of vectors of the electrical field $\mathbf{E}$ (x, y, x) onto the coordinate axes at the position of the object. This also results in excitation of components parallel to the x axis. Angles within the xy plane will be noted as ϕ and those within the xz plane as Θ. Due to the dependance on E^2, different products of $\sin^2$ and $\cos^2$ functions will occur. Additional corrections due to the Fresnel equation, which have to be considered at the transition of light into media of different refractive index, are taken into account by a set of functions $f_{i,j}$, where $i = x, y, z$ and $j = x, y, z$. Differences of the intensity of the exciting light within the cross-section of the beam are represented by the intensity distribution function $L(x, y)$.

The aperture angles ϑ, φ at the position of the object in a different medium are to be calculated from the aperture angles Θ, ϕ in air. Using the focal length of the objective, $L(x, y)$ can be transformed into $L(\Theta, \phi)$, leading to the transformation matrix A:

$$(A) \cdot \begin{pmatrix} 0 \\ i_y \\ i_z \end{pmatrix} = \begin{pmatrix} I_x \\ I_y \\ I_z \end{pmatrix},$$

with $(A) =$

$$\begin{pmatrix} 0 & \int L(\Theta,\phi) f_y(\Theta,\phi) \sin^2\varphi \cos^2\vartheta \, d\Theta d\phi & \int L(\Theta,\phi) f_z(\Theta,\phi) \sin^2\vartheta \cos^2\varphi \, d\Theta d\phi \\ 0 & \int L(\Theta,\phi) f_y(\Theta,\phi) \cos^2\varphi \, d\Theta d\phi & \int L(\Theta,\phi) f_z(\Theta,\phi) \sin^2\vartheta \sin^2\varphi \, d\Theta d\phi \\ 0 & \int L(\Theta,\phi) f_y(\Theta,\phi) \sin^2\vartheta \sin^2\varphi \, d\Theta d\phi & \int L(\Theta,\phi) f_z(\Theta,\phi) \cos^2\vartheta \, d\Theta d\phi \end{pmatrix}.$$

The integrations have to be carried out over all aperture angles. For most of the applications, an elliptical focus has to be considered as indicated in Fig. 3 by broken lines.

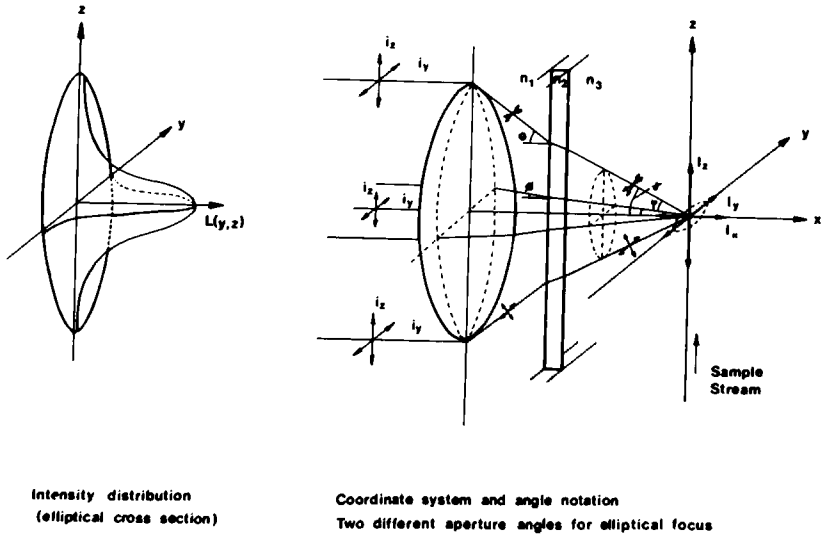

FIGURE 3 Coordinate system and angle notation for the numerical correction. A light beam with a Gaussian intensity distribution (left) passes the intrance aperture of the focusing lens system (solid line), which may as well have an elliptical cross section (broken line). Changes of the refractive index along the optical axis (x axis) are indicated by n_1, n_2 and n_3. The sample flow is along the z axis. The elliptical aperture as indicated forms an elliptical focus at the origin, the long axis of which is parallel to the y axis. The angle notation Θ and ϕ refers to air as medium, ϑ and φ to a medium of a higher refractive index.

Employing an elliptical focus in the epi-configuration, the main axes of the ellipse are oriented parallel to the axes of the coordinate system to simplify further calculations. The aperture angle ϕ parallel to the short main axis of the ellipse (i.e., parallel to the y axis of the optical system [see Fig. 3]) can be considered as very small in a line focus ($\phi < 2.5°$ in the experimental set-up). Therefore, $\cos^2\phi = 1$ and $\sin^2\phi = 0$ is taken as approximation. The transformation matrix in the case of a line focus follows as:

$$A^* = \begin{pmatrix} 0 & 0 & \int L(\Theta) f_z(\Theta) \sin^2\vartheta \, d\Theta \\ 0 & \int L(\Theta) f_y(\Theta) \, d\Theta & 0 \\ 0 & 0 & \int L(\Theta) f_z(\Theta) \cos^2\vartheta \, d\Theta \end{pmatrix}.$$

The intensity $L(\Theta)$ of the exciting light has been measured in our experimental set-up (TEM_{00}-operation) to follow a Gaussian distribution. Every individual laser should be checked for this condition.

For the numerical calculation of the coefficients of the transformation matrix (A^*), second order polynomial functions are taken as approximation for the Fresnel-equations. For a numerical aperture of NA = 0.6 (i.e., Θ_{max}) for example, as used in our systems (10, 11), the transformation matrix for the excitation finally is:

$$(A^*) = \begin{pmatrix} 0 & 0 & 0.010 \\ 0 & 0.410 & 0 \\ 0 & 0 & 0.402 \end{pmatrix}.$$

Note that (A^*) does not turn out to be a diagonal matrix. After normalization the components

of the excitation and adjusting the electrical vector perpendicular to the long axis of the focus ellipse (Fig. 3), the intensity I is:

$$\begin{pmatrix} I_x \\ I_y \\ I_z \end{pmatrix} = \begin{pmatrix} 0.024 \\ 0.050 \\ 0.924 \end{pmatrix} \quad \text{for} \quad \mathbf{i}_{0z} = \begin{pmatrix} 0 \\ 0 \\ 1 \end{pmatrix},$$

if the electrical vector is parallel to the long axis of the focus ellipse:

$$\begin{pmatrix} I_x \\ I_y \\ I_z \end{pmatrix} = \begin{pmatrix} 0.001 \\ 0.950 \\ 0.049 \end{pmatrix} \quad \text{for} \quad \mathbf{i}_{0y} = \begin{pmatrix} 0 \\ 1 \\ 0 \end{pmatrix}.$$

Emission Corrections

The fluorescence intensities in the observation plane are noted as:

$$\mathbf{I}_{\text{Obs}} = \begin{pmatrix} 0 \\ I_{\text{Obs},y} \\ I_{\text{Obs},z} \end{pmatrix},$$

the emitted intensities at the location of the object as:

$$\mathbf{I}_{em} = \begin{pmatrix} I_{\text{em},x} \\ I_{\text{em},y} \\ I_{\text{em},z} \end{pmatrix}.$$

Observing along the x axis and assuming an ideal polarization of the exciting light at the object position,

$$\mathbf{I} = \begin{pmatrix} 0 \\ 0 \\ 1 \end{pmatrix},$$

the degree of polarization is defined as:

$$p = \frac{I_{em,z} - I_{em,y}}{I_{em,z} + I_{em,y}},$$

and the emission anisotropy (14) as:

$$r = \frac{I_{em,z} - I_{em,y}}{I_{em,z} + 2\,I_{em,y}}.$$

If one considers an arbitrary polarization for the exciting beam, i.e.,

$$\mathbf{I} = \begin{pmatrix} I_x \\ I_y \\ I_z \end{pmatrix},$$

the degree of polarization of the emitted fluorescence is:

$$\begin{pmatrix} I_{em,x} \\ I_{em,y} \\ I_{em,z} \end{pmatrix} = k \cdot \begin{pmatrix} I_x & I_y & I_z \\ I_y & I_z & I_x \\ I_z & I_x & I_y \end{pmatrix} \cdot \begin{pmatrix} 1+p \\ 1-p \\ 1-p \end{pmatrix}, \tag{1}$$

where k = normalization factor.

An equivalent set of functions can be derived for the emission anisotropy r. The effect caused by the nonzero aperture can be treated equivalent to the excitation case. The observed intensities I_{Obs} are related to the actual emitted intensities by:

$$(B) \cdot \begin{pmatrix} I_{em,x} \\ I_{em,y} \\ I_{em,z} \end{pmatrix} = \begin{pmatrix} 0 \\ I_{\text{Obs},y} \\ I_{\text{Obs},z} \end{pmatrix} \tag{2}$$

$$(B) = \begin{pmatrix} 0 & 0 & 0 \\ \int \cos^2\vartheta \sin^2\varphi \, \mathrm{d}\vartheta\mathrm{d}\varphi & \int \cos^2\varphi \, \mathrm{d}\vartheta\mathrm{d}\varphi & \int \sin^2\vartheta \sin^2\varphi \, \mathrm{d}\vartheta\mathrm{d}\varphi \\ \int \sin^2\vartheta \cos^2\varphi \, \mathrm{d}\theta\mathrm{d}\varphi & \int \sin^2\vartheta \sin^2\varphi \, \mathrm{d}\vartheta\mathrm{d}\varphi & \int \cos^2\vartheta \, \mathrm{d}\vartheta\mathrm{d}\varphi \end{pmatrix},$$

integrating over all angles ϑ, φ in the medium accepted by the lens system. Assuming a circular aperture along the observation pathway, an additional correction of the degree of polarization or emission anisotropy according to the Fresnel-equations can be neglected, because two data sets of two directions of the main excitation polarization are taken for further calculations: (*a*) polarization parallel to the z axis (referred to later as index $i = 1$), (*b*) polarization parallel to the y axis (referred to later as index $i = 2$).

Corrections will be different for both cases if an elliptical aperture is used for excitation. If one considers a_i and b_i as correction coefficients for the degree of polarization p, the observed intensities are related by:

$$\begin{aligned} k_1 I^{(1)}_{\text{Obs},z} &= 1 + a_1 p; \quad k_2 I^{(2)}_{\text{Obs},y} = 1 + a_2 p \\ k_1 I^{(1)}_{\text{Obs},y} &= 1 - b_1 p; \quad k_2 I^{(2)}_{\text{Obs},z} = 1 - b_2 p, \end{aligned} \tag{3}$$

where k_i = normalization factors.

An equivalent set of equations can be derived for the emission anisotropy. The ideal (i.e., zero) aperture, would result in:

$$\begin{aligned} a_i = b_i &= 1 \qquad \text{for } p; \\ a_i = 2;\ b_i &= 1 \qquad \text{for } r. \end{aligned}$$

For a real circular aperture ($\Theta_{\max} = \phi_{\max}$; NA = 0.6), as used in our system:

$$(B) = \begin{pmatrix} 0 & 0 & 0 \\ 0.052 & 0.946 & 0.002 \\ 0.052 & 0.002 & 0.946 \end{pmatrix}.$$

B_{1n} are set to zero, because intensity components along the x axis can not be observed. Eq. 2 with Eq. 1 becomes for this case:

$$\begin{pmatrix} 0 & 0 & 0 \\ 0.052 & 0.946 & 0.002 \\ 0.052 & 0.002 & 0.946 \end{pmatrix} \cdot \begin{pmatrix} I_x & I_y & I_z \\ I_y & I_z & I_x \\ I_z & I_x & I_y \end{pmatrix} \cdot \begin{pmatrix} 1+p \\ 1-p \\ 1-p \end{pmatrix} = \begin{pmatrix} 0 \\ I_{\mathrm{Obs},y} \\ I_{\mathrm{Obs},z} \end{pmatrix}. \tag{4}$$

The matrix I takes care of the corrections for the excitation as mentioned before. The coefficients of Eq. 3 can then be calculated as:

	a_1	a_2	b_1	b_2	
and	0.754	0.797	0.900	0.910	for the determination of p
	1.630	1.695	0.850	0.859	for the determination of r.

The observed polarization is corrected by the equations derived here for aperture effects along the excitation as well as along the emission path taking the influence due to the Fresnel equations, Snell's law and nonuniform intensity distribution of the exciting light into account. The aperture may be considered as circular as well as elliptical. The latter results in $a_1 \neq a_2$ and $b_1 \neq b_2$, as shown above.

Evaluation of the Polarization Histogram

An adjustment for equal sensitivity of both polarization detection channels (including the optical and the electronical part) before every measurement is necessary in a 90° (excitation vs. observation direction) design. However, a precise preadjustment is not necessary for an epi-illumination system. By comparing data of two subsamples taken by two subsequent runs from the same cell suspension, a numerical correction of the data compensates different detector sensitivities.

Fluorescence intensities parallel and perpendicular to the excitation polarization are recorded by a two parameter multichannel analyzer. The polarization of the exciting light is turned by 90° between two subsequent runs. In accordance to the notation used before, the two polarizations of the exciting light will be marked by the indices 1 and 2. Parallel as well as perpendicular fluorescence components from every cell are taken and displayed as a three-dimensional histogram. The X and Y axes represent the intensities of the polarization components, the Z axis the number of cells. A projection of these three-dimensional distributions onto the X, Y plane will result in clublike contour shapes (Fig. 4). A 90° rotation of the excitation polarization results in a histogram rotated with respect to the origin. The angle between the two axes of the distributions is related to the emission anisotropy of the sample. The width of the club is given by the polarization distribution of the sample as well as by the statistical broadening due to the measuring system. In a first order approximation both distributions will be mirror-symmetric. If both detector channels are adjusted to the same sensitivity, the axis of symmetry will coincide with the diagonal in the X, Y plane (Fig. 4). The DC-offset of the electronic signal processing is assumed to be constant. This will be considered in the calculation by shifting the datafield for an equivalent amount. Intensity data, already corrected for the DC-offset, will be represented by X_i and Y_i in accordance with the notation

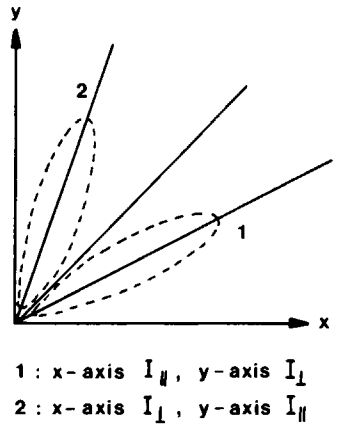

FIGURE 4 Schematic representation of the control map generated during data correction. The clublike shape refers to the projection of a selected contor level of the two parameter histogram on to the XY plane (N is represented along the z axis). Index 1 refers to the first of two subsequent runs, representing $I_{\parallel}$ along the X axis and $I_{\perp}$ along the Y axis. Index 2 refers to the inverse situation. If the detectors are adjusted for the same sensitivity, both projections (broken lines 1 and 2) are mirror symmetric with respect to a diagonal line. The solid lines through 1 and 2 are plotted by the program to control the evaluation of the correction factors by the computer.

of the histogram axes. Different sensitivities of both detectors will be corrected by a gain correction factor g. The histogram representation of the observed values is given by:

$$I^{(i)}_{\mathrm{Obs},z} = X_i$$
$$I^{(i)}_{\mathrm{Obs},y} = g \cdot Y_i. \tag{5}$$

Both subsequent runs are taken from the same sample. Therefore the degree of polarization is expected not to change between both measurements. Using Eqs. 3 and 5 results in:

$$\frac{X_1}{Y_1} \cdot \frac{Y_2}{X_2} = \frac{1 + p(a_1 + a_2) + a_1 a_2 p^2}{1 - p(b_1 + b_2) + b_1 b_2 p^2}. \tag{6}$$

Single beam flow systems do not easily allow the simultaneous detection of the two pairs of data on a single cell. Therefore in a single beam system as used here a mean value for X_1/Y_1 and Y_2/X_2 is needed for the determination of g. However, this can be avoided in a double-beam flow cytometer as described before for internally calibrated particle sizing (10). In this design (10) cells intersect two beams. The direction of the polarization of both beams is oriented perpendicularly. In the case discussed here, Eq. 6 can be solved in good approximation by using the means:

$$\text{for } i = 1: \left(\frac{\overline{X_j}}{\overline{Y_j}}\right) = \frac{\sum_j \frac{X_j}{Y_j} Z(X_j, Y_j) T(X_j, Y_j)}{\sum_j T(X_j, Y_j) Z(X_j, Y_j)}$$

$$\text{for } i = 2: \overline{\left(\frac{Y_j}{X_j}\right)} = \frac{\sum_j \frac{Y_j}{X_j} Z(X_j, Y_j) T(X_j, Y_j)}{\sum_j T(X_j, Y_j) Z(X_j, Y_j)}, \tag{7}$$

where $T(X_j, Y_j) = (X_j + Y_j)^W$, $Z(X_j, Y_j)$: number of particles at the histogram-location X_j, Y_j, W is a weighting exponent, which is 0 if all intensities contribute equally. $W \neq 0$ allows an over- or underweighting of higher intensity of cells or particles. Using Eq. 6, an average p_o is calculated. With Eqs. 3 and 5 a measure of the symmetry of the detection system, expressed as g, is given. For every location within the X–Y data plane is:

$$p(X_{1,j}; Y_{1,j}) = \frac{X_{1,j} - gY_{1,j}}{b_1 X_{1,j} + g a_1 Y_{1,j}}$$

and

$$p(X_{2,j}; Y_{2,j}) = \frac{gY_{2,j} - X_{2,j}}{g b_2 Y_{2,j} + a_2 X_{2,j}}.$$

The weighted numbers $M = Z(X_j, Y_j) \cdot T(X_j, Y_j)$ for every p-value are added to evaluate a p-histogram. If only locations in the X–Y data plane very close to the origin, i.e., representing small intensities have accumulated large numbers, the histogram, of the degree of polarization shows a structure, which is due to the limited resolution of the data matrix (usually 32 × 32 or 64 × 64). A calculation of the degree of polarization of every particle or cell before data storage in a multichannel analyzer would allow a higher resolution of the p-histogram. Using the internal calibration as described here, a precalculation will be possible only in a double beam detection system.

The accuracy in the determination of p-values is given by the resolution of the 32 × 32 data matrix and is dependent on the distance of the histogram locations from the origin due to the calculations leading to the p-values. It is of advantage therefore to adjust the photodetector amplifiers in that way to allow the maximum number of cells to accumulate at a certain distance from the origin.

RESULTS AND DISCUSSION

For test purposes, particles or cells showing the extremes of highly polarized or unpolarized fluorescence emission are most helpful. Fluorescent latex microspheres, widely used for testing flow cytometry equipment exhibit little dye mobility and therefore a high degree of polarization. The particles used showed an extremely wide range of fluorescence intensities and the suspension a very high fraction of debris. Results of a measurement of fluorescent latex microspheres are shown in Fig. 5 *a*. The left part is a control map of intensities parallel and perpendicular to the polarization of the exciting light equivalent to the schematic representation in Fig. 4. The peak numbers of the histogram are found on the low intensity end of the intensity scale. To generate the control map, two contour levels of the histogram are selected during program execution. Only those positions, which have accumulated cell numbers between the two limits, are marked in the X, Y plane. The two subsequent runs of the

same sample with the direction of polarization of the exciting light being rotated by 90° are indicated by crosses and dots. This representation gives a rough impression of the profile of the three dimensional histogram. Both histograms are typically based on at least 10^4 cells or particles measured. Crosses and dots therefore do not mark the data set of a single cell, but represent the location of a given number of cells within the three-dimensional histogram as projected onto the parameter plane. Data are corrected for the DC-offset at this point only.

Using the display mode, the two runs are expected to be symmetric with respect to the 45° axis. Asymmetries by improper balance of amplifier sensitivities are corrected by the computer program as described before. The two straight lines indicate the means determined by the program calculating the g factors. Additional corrections for excitation asymmetries and aperture effects are implemented in the calculation of the corrected polarization histogram shown on the right hand side of Fig. 5. It is obvious that the anisotropy of those locations in the histogram close to the origin can only be computed with the lower accuracy compared to those representing high intensities. The calculated mean value for the polarization of fluorescent Latex microspheres was found as $p = 0.409 \pm 0.067$. From the limited resolution of the 32 × 32 matrix and because the highest numbers are found close to the origin, one expects a rather large standard deviation exceeding $p = 0.5$ by the tail of the distribution which is due to the relatively high error contribution of the low intensity part of the histogram. A variation of the polarization with fluorescence intensity has not been found. In Fig. 6, a polarization measurement on intracellular DNA stained with ethidium bromide and mithramycin after fixation is shown. In contrast to the data on Latex microspheres, the largest numbers in the histogram are found at high intensities. Therefore the standard deviation of the p histogram is considerably smaller. A highly depolarized fluorescence emission is found in green algae. Due to fast energy transfer within the chloroplasts, the fluorescence emission of chlorophyll exhibits only a very small degree of polarization. Low excitation power and suboptimal excitation frequency (10 mW at 441 nm) resulted in low fluorescence intensities, a low signal-to-noise ratio and subsequently large standard deviation.

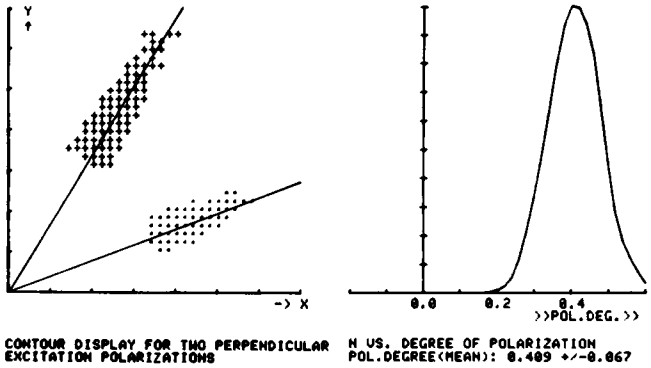

FIGURE 5 Fluorescence polarization measurements on fluorescent Latex microspheres. (left) Control map of the projection of a selected contour level of the three-dimensional histogram on to the XY plane. The two paired runs with different directions of the excitation polarization are indicated by dots and crosses. (right) Polarization histogram corrected for depolarizing effects and calculated from the uncorrected histogram (left).

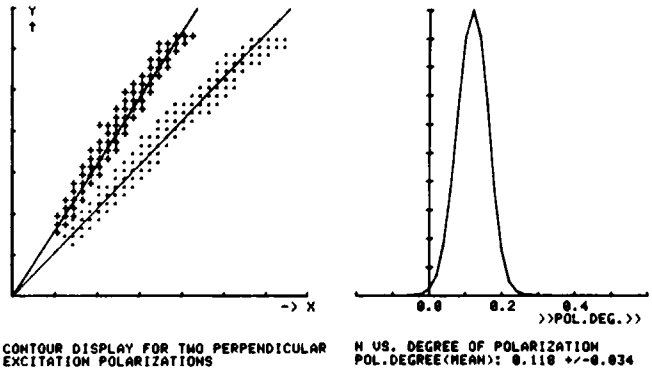

FIGURE 6 Fluorescence polarization measurements on intracellular DNA after fixation and staining with ethidium bromide and mithramycin. Same data representation as in Fig. 5.

Fig. 6 shows the data of fluorescence polarization measurements at the alga *Chlorella vulgaris*. Fluorescence was detected at wavelengths longer than 665 nm. The control map shows the overlap of data of both runs (crosses and dots). The contour level cut indicates that the maxima of both histograms are located close to the origin, i.e., at low fluorescence intensities, and therefore large error contributions are expected. A two parameter histogram with large numbers close to the origin necessarily leads to a structure of the polarization histogram due to the limited resolution at low intensities. This is clearly to be seen in the right-hand part of Fig. 7. Taking the large standard deviation of ± 0.159 into account, the fluorescence emission of *C. vulgaris* is totally depolarized.

Although these particles and cells are not necessary for alignment in our system, algae might well be used as test objects for the adjustment of different polarization devices. The results further indicate that the formalism derived here for the calculation of p and r seems to take care of all significant depolarizing contributions during the measurement.

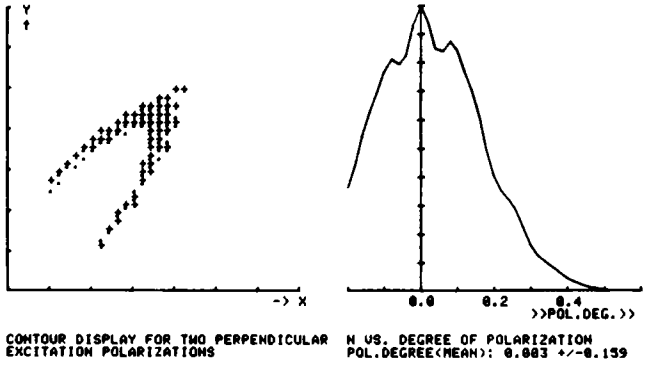

FIGURE 7 Fluorescence polarization measurements on the alga *C. vulgaris*. (left) Control map of the projection of a selected contour level of the three-dimensional histogram on to the XY plane. The two paired runs are indicated by dots and crosses. (right) Corrected polarization histogram calculated from the raw data. Most of the cells exhibit very low fluorescence intensities, resulting in structure of the distribution of polarization.

Experiments on human lymphocytes with and without stimulation are discussed in more detail elsewhere (3, 13).

SUMMARY

An epi-illumination system for detecting the polarization of emitted fluorescence in flow cytometry is introduced. Detecting fluorescence polarization effects in the backward direction is more favorable than a 90° arrangement because anisotropic effects in the optical system as well as improper alignments of the electronics are compensated by pairs of experiments with changed polarization of the exciting light. In addition, internal structure and complexity of biological particles may cause secondary effects which may play an unexpectedly important role in high intensity laser excitation.

A formalism has been derived to calculate depolarizing effects along the excitation as well as the emission path. The influence of a large aperture, the cross-section of which may be elliptical, and a nonuniform intensity distribution of the excitation beam are considered for the excitation beam as well as the influences of the Fresnel equations and Snell's law. Two sets of fluorescence data, generated by two subsequent runs on the same sample, but with different excitation polarizations, allow the numerical correction of mismatches of the two detection channels. This eliminates a precise preadjustment for equal response of the detector systems by additional test runs. The system performance has been tested by taking data of fluorescent microspheres as well as green algae. Both objects may well be used for the adjustment of fluorescence polarization equipment of different principle design.

Received for publication 12 September 1979 and in revised form 7 January 1980.

REFERENCES

1. ARNDT-JOVIN, D. J., and T. M. JOVIN. 1976. Cell Separation Using Fluorescence Emission Anisotropy; Membranes and Neoplasia; New Approaches and Strategies. A. R. Liss Inc., New York. 123–136.
2. AXELROD, D. 1976. Carbocyanine dye orientation in red cell membrane studied by microscopic fluorescence polarization. *Biophys. J.* **26**:557–573.
3. BEISKER, W., W. G. EISERT, T. M. FLIEDNER, W. HARTMANN, and E. SACKMANN. 1980. Flow cytometric measurements of fluorescence depolarization in human lymphocytes: differences in cells from patients with and without neoplasia. *Br. J. Cancer.* In press.
4. CERCEK, L., B. CERCEK, and CH. OCKEY. 1973. Structuredness of cytoplasmic matrix and michaelis-menten constants for the hydrolysis of FDA during the cell cycle in Chinese hamster ovary cells. *Biophysik.* **10**:187–194.
5. CERCEK, L., B. CERCEK, and CH. OCKEY. 1978. Fluorescein excitation and emission polarization spektra in living cells. *Biophys. J.* **23**:395–405.
6. CHAN, S. S., D. J. ARNDT-JOVIN, and T. M. JOVIN. 1979. Proximity of lectin receptors on the cell surface measured by fluorescence energy transfer in a flow system. *J. Histochem. Cytochem.* **27**:56–64.
7. CRAM, L. S., D. J. ARNDT-JOVIN, B. G. GRIMWADER, and T. M. JOVIN. 1979. Fluorescence polarization and pulse width analysis of chromosomes by a flow system. *J Histochem. Cytochem.* **27**:445–453.
8. DALE, R. E., and R. K. BAUER. 1971. Concentration depolarization of the fluorescence of dyestuffs in viscous solution. *Acta Physica Polonica.* **A40**:853–882.
9. EISERT, W. G. 1979. Cell differentiation based on absorption and scattering. *J. Histochem. Cytochem.* **27**:404–409.
10. EISERT, W. G., and M. NEZEL. 1978. Internal calibration to absolute values in flough through particle size analysis. *Rev. Sci. Instrum.* **49**:1617–1621.
11. EISERT, W. G., R. OSTERTAG, and E.-G. NIEMANN. 1975. Simple flow microphotometer for rapid cell population analysis. *Rev. Sci. Instrum.* **46**:1021–1024.

12. EPSTEIN, M., A. NORMAN, D. PINKEL, and R. UDKOFF. 1977. Flow system fluorescence polarization measurements on fluorescein diacetate-stained EL 4 cells. *J. Histochem. Cytochem.* **25**:821–826.
13. HARTMANN, W., W. BEISKER, and W. G. EISERT. Fluorescence Polarization Measurements on Human Lymphocytes. *Acta Pathologica et Microbiologica Scandinavica.* In press.
14. JABLONSKI, A. 1960. On the notation of emission anisotropy. *Bull. Acad. Polon. Sci. Ser. Sci. Math. Astron. Phys.* **8**:259–264.
15. JARRY, J. P., and L. MONNERIE. 1978. Orientation and molecular dynamics of uniaxial polymers. I. Theory of fluorescence polarization. *J. Polymer Sci.* **16**:443–455.
16. JARRY, J. P., P. SERGOT, C. PAMBRON, and L. MONNERIE. 1978. A fluorescence polarization apparatus for the simultaneous measurement or orientation and mobility in uniaxial media. *J. Phys. E. Sci. Instrum.* **11**:702–706.
17. KRATOHVIL, J. P., M.-P. LEE, and M. KERKER. 1978. Angular distribution of fluorescence from small particles. *Appl. Optics.* **17**:1978–1980.
18. KREUTZMANN, H., T. M. FLIEDNER, H. J. GALLA, and E. SACKMANN. 1978. Fluorescence-polarization changes in mononuclear blood leucocytes after PHA incubation: differences in cells from patients with and without neoplasia. *Br. J. Cancer.* **37**:797–805.
19. LEE, E.-H., R. E. BRENNER, J. B. FENN, and R. K. CHANG. 1978. Angular distribution of fluorescence from monodispersed particle. *Appl. Optics.* **17**:1980–1982.
20. LINDMO, T., and H. B. STEEN. 1977. Flow cytometric measurement of the polarization of fluorescence from intracellular fluorescein in mammalian cells. *Biophys. J.* **18**:173–187.
21. PRICE, G. B., M. J. MCCUTCHEUN, W. B. TAYLOR, and R. G. MILLER. 1977. Measurement of cytoplasmic fluorescence depolarization of single cells in a flow system. *J. Histochem. Cytochem.* **25**:597–600.
22. UDKOFF, R., and A. NORMAN. 1979. Polarization of fluorescein fluorescence in single cells. *J. Histochem. Cytochem.* **27**:49–55.
23. WEBER, G. 1952. Polarization of the fluorescence of macromolecules. *Biochemistry.* **51**:145–155.
24. ZINSLI, P. E. 1978. Correction for finite apertures in fluorescence polarization measurements. *J. Phys. E Sci. Instrum.* **11**:17–19.